Harmonic Stability in Power Electronic Based Power Systems: Concept, Modeling, and Analysis

Xiongfei Wang, *Senior Member, IEEE*, Frede Blaabjerg, *Fellow, IEEE*

***Abstract*—The large-scale integration of power electronic based systems poses new challenges to the stability and power quality of modern power grids. The wide timescale and frequency-coupling dynamics of electronic power converters tend to bring in harmonic instability in the form of resonances or abnormal harmonics in a wide frequency range. This paper provides a systematic analysis of harmonic stability in the future power-electronic-based power systems. The basic concept and phenomena of harmonic stability are elaborated first. It is pointed out that the harmonic stability is a breed of small-signal stability problems, featuring the waveform distortions at the frequencies above and below the fundamental frequency of the system. The linearized models of converters and system analysis methods are then discussed. It reveals that the linearized models of ac-dc converters can be generalized to the harmonic transfer function, which is mathematically derived from linear time-periodic system theory. Lastly, future challenges on the system modeling and analysis of harmonic stability in large-scale power electronic based power grids are summarized.**

***Index Terms*—harmonic stability, damping, power electronics, power systems, resonance.**

I. Introduction

THE legacy power grids that are dynamically dominated by electrical machines are evolving as power electronic based power systems, driven by the large-scale adoption of electronic power converters for renewable generations and energy-saving applications [1], [2]. This radical transformation paves the way towards modern power grids with high flexibility, sustainability and improved efficiency, yet it also poses new challenges to the stability and power quality of the power system [3].

Power converters are commonly equipped with a multiple-timescale control system for regulating the current and power exchanged with the power grid [4]. The wide timescale control dynamics of converters can result in cross couplings with both the electromechanical dynamics of electrical machines and the electromagnetic transients of power networks, which may lead to oscillations across a wide frequency range [5], [6]. This issue becomes severe with the ever-increasing penetration of power electronic based systems. A number of incidents have been reported with the grid integration of renewables and high-speed trains [7]-[9], where the undesired harmonics, inter-harmonics, or resonances caused disruption to the power supply.

There have been growing interests in identifying the causes of abnormal harmonics and resonances in the power electronic based power systems. It is found that the small-signal dynamics of converters tend to introduce a negative damping in the power system, which may be in different frequency ranges, depending on both the specific controllers of converters and power system conditions [10]-[15]. For instance, the time delay of the digital control system used with converters adds a negative damping in the high frequency range [10], while the Phase-Locked Loop (PLL) of inverters [11], [12], or the constant power control of rectifiers [13], brings a negative damping in the low frequency range. Furthermore, the frequency-coupling mechanism of the switching modulation and the sampling process can also lead to a negative damping in the high frequency range [14], [15]. The negative damping tends to destabilize the natural frequencies of the power system, e.g. the LC resonance frequencies of power filters and cables, provoking the so-called harmonic instability problem, which is also named as the resonance instability [16]. Moreover, the harmonic instability phenomena will further turn into the critically damped resonances or under-damped (inter-) harmonics, if the net damping of the electrical system is non-negative [17], [18].

A wide variety of linearized models of power converters can be used for harmonic stability analysis [19]-[24]. These models fall into two categories, depending on the considered operating points (or trajectories) of the converter. The first category is the averaged model based on the moving average operator, where only the dc operating point is considered, whereas the switching modulation process is implicitly neglected by averaging system variables over one switching period. Thus, the moving averaged model can only predict the converter dynamics below half the switching frequency [19], [20]. The second category is the multiple-frequency model in different forms, e.g. the describing function model [21], the multiple-frequency averaging model [22], [23], and the Harmonic State-Space (HSS) model [24]. All the multiple-frequency dynamic models are developed based on the principles of harmonic balance and describing function [23], and the Linear Time-Periodic (LTP) system theory [24]. Those models capture the frequency coupling dynamics of multiple time-periodic operating trajectories, and thus provide accurate assessments on the harmonic stability, yet their Multiple-Input Multiple-Output (MIMO) nature tends to complicate the system stability analysis with high computational power as a demand.

There are two approaches for the system-level analysis of harmonic stability. The first method is the eigenvalue analysis based on the state-space model in the time-domain [25], which is commonly used to analyze electromechanical oscillations in the legacy power grids. The superior features of this method are the identifications of the oscillation modes and the participation factors of system variables [26]. Yet, due to the wide timescale dynamics of converters, the electromagnetic dynamics of power networks have to be included in the state-space model, which significantly increases the system order and thus requires high computational power [27]. The second type is in the frequency-

domain, which is also named as the impedance-based analysis. In the method, the dynamics of converters are extracted at their terminals by using frequency-domain transfer functions, which are then translated to electrical impedances, and thus the system stability can be analyzed by means of the electric circuit theory [28]. The impedance-based approach was earlier developed to analyze the interactions of converters in dc power systems [29]. Its main advantage lies in the black-box modeling of converters, which enables to predict the system dynamics without the prior knowledge of system parameters. Moreover, the impedance-based method predicts the system stability at the terminals of the converters and thus the contribution of each converter to the system stability can be identified. However, it may also lead to an inaccurate stability prediction when there are Right Half-Plane (RHP) poles hidden in the measured or the estimated impedances [30], [31].

This paper elaborates first the harmonic stability concept and phenomena based on the converter-grid interaction. The unique features of the harmonic stability problem in comparison to the conventional small-signal stability issues are pointed out. Then, linearized modeling methods of converters and system analysis tools for the harmonic stability of converter-based systems are discussed. Lastly, challenges on the system-level modeling and analysis of the harmonic stability conclude this paper.

II. Harmonic Stability Concept and Phenomena

This section presents first a historical review of the harmonic stability in traditional ac-dc power systems, and then elaborates the basic concept and phenomena of harmonic stability in future power electronic based power grids.

A. Historical Review

The harmonic stability problem is not new, and it was earlier reported in the commissioning stage of the High Voltage Direct Current (HVDC) Cross-Channel link in 1961 [32]. That HVDC system was based on the Line-Commutated Converters (LCCs), where the voltage distortion caused by a high grid impedance, i.e. a low Short-Circuit Ratio (SCR) grid, leads to asymmetric firing angles for the LCC, which consequently distorts the grid current with the unexpected harmonics, and forms a positive feedback loop with the grid impedance [33], [34]. The harmonic instability of LCC-HVDC system can be exaggerated by the core saturation of the converter transformer [35]. A second-order harmonic instability resulting from the transformer core saturation has been well discussed in [36].

It is worth mentioning that the characteristic of the ac system impedance is important for the harmonic stability of the LCC-HVDC systems [34]. The system is more prone to the harmonic instability in the high-impedance (the low SCR) grid, where the high voltage harmonics are introduced at the input of the firing-angle control system, and the frequency-coupling nature of the firing angle control distinguishes the harmonic instability from the instability of low-frequency control loops [33]. Moreover, the frequency transformation of ac-dc converters translates the oscillation component (f_{dc}) at the dc-side into two components of the frequencies $f_1 \pm f_{dc}$ at the ac-side, where f_1 is the grid fundamental frequency. These two components can be seen as the sideband components of the fundamental frequency, which may also cause the harmonic instability when interacting with the ac system impedance.

B. Harmonic Stability Concept

Unlike traditional ac-dc power systems, the self-commutated Voltage-Source Converters (VSCs) are dominantly found in the present power electronic based power systems, e.g. renewable power plants, traction power networks, and microgrids. In these systems, the harmonic stability have more different forms than the LCC-HVDC systems, due to the multiple-timescale control dynamics of VSCs [3]-[5].

Fig. 1 illustrates a general diagram of a grid-connected VSC and the equivalent circuits. Ideally, the VSC can be equivalent as a current source, as shown in Fig. 1(b), where the passive LC resonance can be triggered by either the current source (parallel resonance) or the grid voltage (series resonance). However, due to the finite bandwidth of the control system of the VSC, there is a control output admittance added in parallel with the current source, as shown in Fig. 1(c). Depending on the used controller, the control output admittance may have a positive, zero, or even negative real part in different frequency ranges, which leads to the damped/under-damped, critically damped, or exponentially amplified resonances in the VSC system. Hence, the harmonic instability differs from the passive harmonic resonance in its dependence on the control dynamics of the converters.

Fig. 2 establishes a mapping between the forms of harmonic instability to the cascaded control system of the VSC, including the outer loops for the Direct Voltage Control (DVC) and the Alternating Voltage Control (AVC), the PLL for synchronizing the VSC to the grid, and the inner Alternating Current Control (ACC) loop. These control loops are designed with the different bandwidths, which interact with the grid impedance, leading to the harmonic instability phenomena from the sub-synchronous frequencies to multiple kilohertz (kHz).

Differing from the LCC, there are two sidebands (frequency-coupling dynamics) generated from VSCs. The first sideband is of the fundamental frequency, which is caused by the frequency transformation mechanism of the dc-ac conversion and of the used Park (*dq*-) transformation [5]. The second sideband is of the switching frequency of the VSC or of the Nyquist frequency

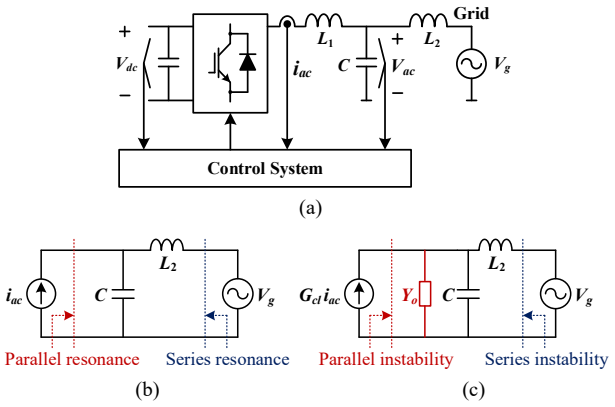

Fig. 1. General diagram of a grid-connected VSC and its equivalent circuit. (a) Grid-connected VSC. (b) Ideal current source equivalent. (c) Equivalent circuit with control output admittance.

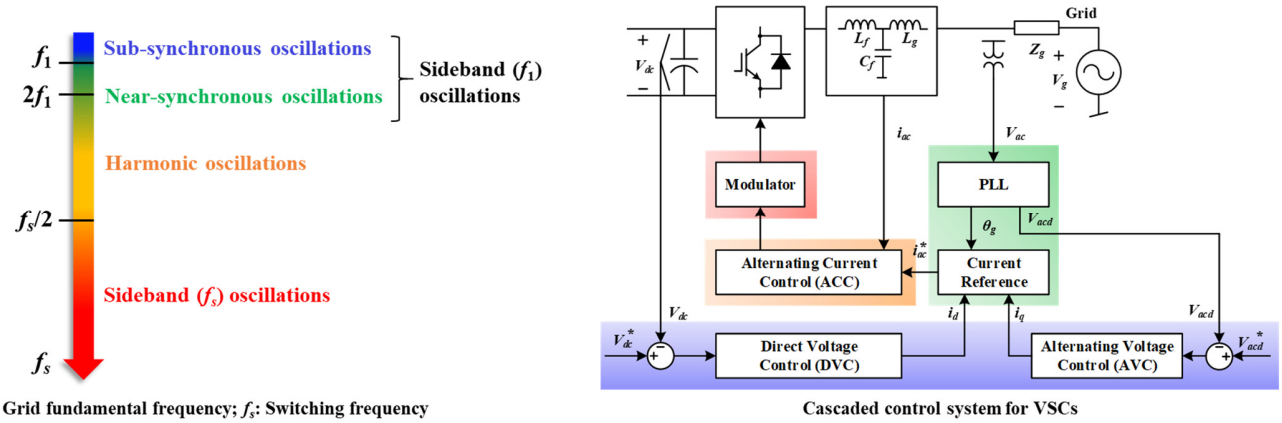

Fig. 2. A mapping between the forms of harmonic instability and the specific control loops of VSCs.

of the digital control system, resulting from the Pulse-Width Modulator (PWM) or the sampling process [14]. Consequently, two forms of sideband-harmonic instability can be provoked in the VSC-based power system:

1) Sideband oscillations (f_1) of the fundamental frequency, which are due to the asymmetrical dynamics of the PLL and outer control loops in the *dq*-frame [5]. For VSCs operating as inverters, the PLL introduces a negative damping that only affects the *q*-axis dynamics, since only the *q*-axis voltage is controlled within the PLL for the phase detection [11], [12]. In contrast, the DVC adds a negative damping on the *d*-axis dynamic when the VSCs operate as rectifiers owing to the constant power load characteristic at the dc-side [13]. The asymmetrical oscillations at the frequency f_{dq}, either on the *q*-axis or on the *d*-axis, can thus be brought in the *dq*-frame, which causes the sideband oscillations at the frequencies $f_1 \pm f_{dq}$ in the stationary phase domain [11]. The occurrence of this asymmetrical oscillation is dependent on the strength of the ac system. The power grid with a low SCR is more prone to the asymmetrical oscillation [12]. It is worth noting that the frequency component, $f_1 - f_{dq}$, becomes a sub-synchronous oscillation, when the oscillation frequency f_{dq} is below $2f_1$, and it is in the positive sequence for $f_1 - f_{dq} > 0$, and in the negative sequence for $f_1 - f_{dq} < 0$. In the case that the sideband oscillations $f_1 \pm f_{dq}$ are both in the positive-sequence, they cannot be captured by the sequence-domain model [50]. The sub-synchronous oscillation component can further excite the natural frequencies of the shaft of the electrical machines, leading to the torsional oscillations [37]. When $f_{dq} < 2f_1$, the frequency component, $f_1 + f_{dq}$, leads to a near-synchronous oscillation around $2f_1$ [5].

2) Sideband oscillations (f_s) of the switching frequency, which are caused by the frequency-coupling dynamics of the PWM and the sampling process. It has been recently shown that the small-signal (sinusoidal) perturbation component introduces an additional sideband in the low frequency range [14], [38]. The lower frequency component of the small-perturbation-induced sideband may interact with the inner ACC loop, resulting in the sideband-harmonic instability, which has been found in the paralleled VSCs with the asynchronous carriers [14]. A similar harmonic instability phenomenon has also been seen in the dc systems, where the interconnected dc-dc converters with different switching frequencies can interact with each other, resulting in beat frequency oscillations [39]. The other case is the negative damping added above the Nyquist frequency by the ACC loop with the reduced time delay [15], and the negative damping may destabilize the LC resonance frequency above the Nyquist frequency. This sideband oscillation is due to the frequency coupling dynamics of the sampling process.

In addition, the harmonic instability may also result from the wideband inner ACC loop, where the time delay can also add a negative damping below the Nyquist frequency, which then can destabilize the system with the harmonic-frequency oscillations [10], [17]. Differing from the sideband-harmonic instability, no frequency-coupling small-signal dynamics are involved in this case. Yet, the inherent nonlinearities of the ACC loop, such as the anti-windup of the controller and the over-modulation of the PWM tend to dampen the exponentially amplified oscillation as (inter-) harmonics and resonances.

Hence, the harmonic stability is basically a breed of small-signal stability, yet it features the waveform distortions at the frequencies above and below the grid fundamental frequency, which may come from the interactions of the wideband control loops [17], or result from the frequency-coupling dynamics of the fundamental frequency [11], and the switching and Nyquist frequencies [14], [15].

C. Harmonic Instability Phenomena

To see the phenomena of harmonic instability in the power-electronic-based power system, a test setup has been built with three paralleled VSCs and a Chroma grid simulator, as shown in Fig. 3. Fig. 3(b) depicts the circuit schematics of the system. The paralleled VSCs are equipped with identical controller and circuit parameters, and their carrier waves within the PWM are intentionally synchronized, except in the case shown in Fig. 6. The constant dc-link voltages powered by the separate dc power supplies are configured with three paralleled VSCs in order to avoid the common mode circulating current.

Fig. 4 shows the measured waveforms for the dynamic effect of the PLL on three paralleled VSCs. Two operating scenarios with the different SCRs are tested, and the same PLL is used in

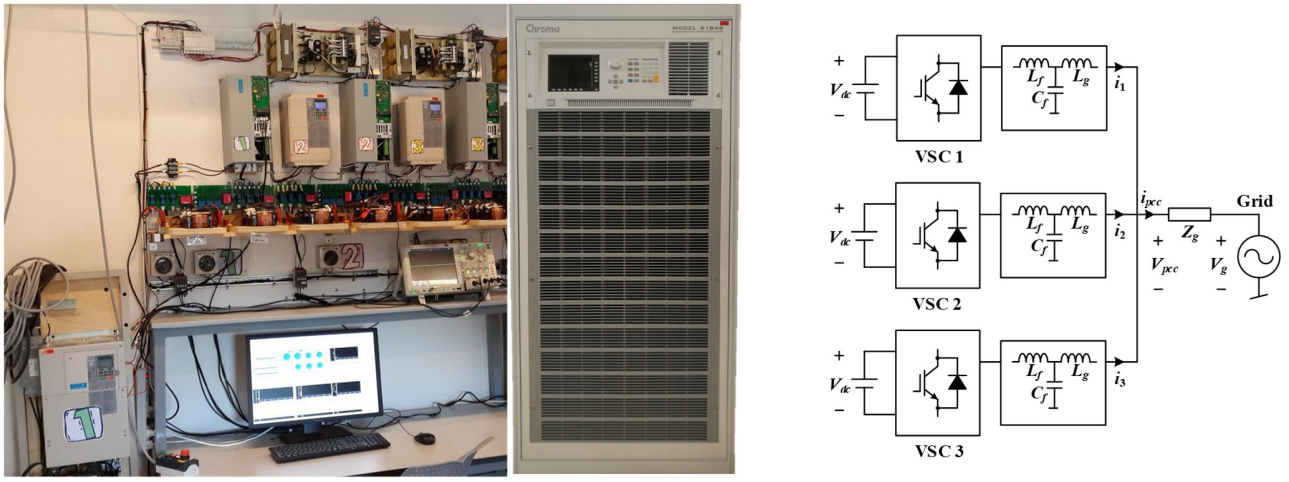

(a) (b)

Fig. 3. A power-electronic-based power system with three paralleled inverters and a grid power supply. (a) Hardware picture. (b) Circuit schematics.

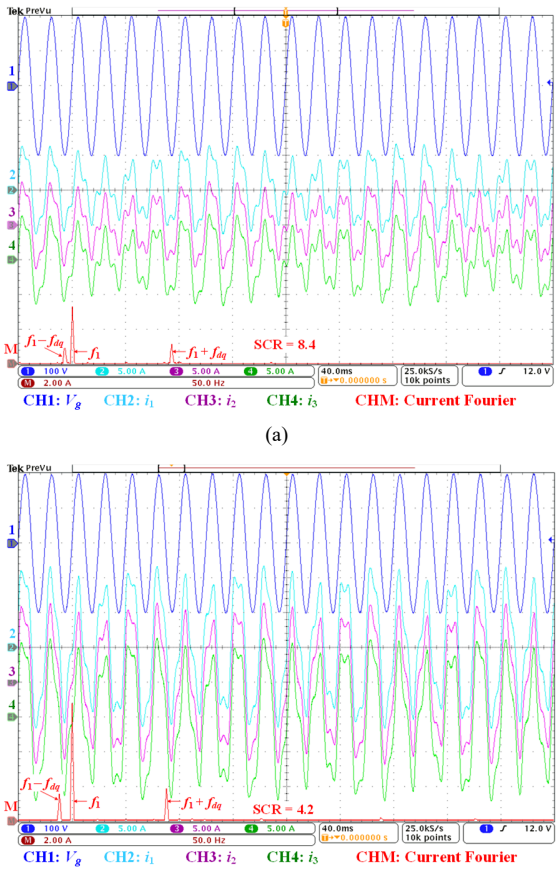

(a)

(b)

Fig. 4. Measured waveforms for the sideband (f_1) harmonic instability induced by the PLL dynamic with the different Short-Circuit Ratios (SCRs). (a) SCR = 8.4. (b) SCR = 4.2.

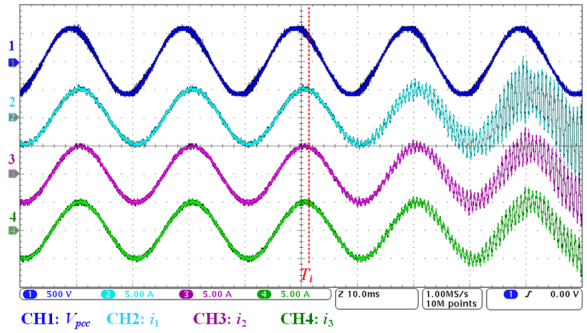

Fig. 5. Measured waveforms for the harmonic instability resulted from the current control interactions of the paralleled VSCs, where the bandwidth of the Alternating Current Control (ACC) loop is increased at the time T_i.

both cases. The per-phase output voltage of the grid simulator and per-phase VSC currents with the Fourier spectra are shown. It is evident that the VSC currents are distorted with two inter-harmonic components even under the sinusoidal grid condition. The two abnormal harmonics are at the frequencies above and below the fundamental frequency, which indicate the sideband oscillations of the fundamental frequency: $f_1 \pm f_{dq}$, where f_{dq} is the PLL-induced oscillation frequency in the dq-frame [12]. As the near-synchronous oscillation frequency, $f_1 + f_{dq}$, is above $2f_1$, the sub-synchronous oscillation is in the negative sequence, i.e. $f_1 - f_{dq} < 0$. By comparing Fig. 4(b) and Fig. 4(a), it is also noted that given a PLL bandwidth, the reduced SCR shifts the resulting sideband oscillations to the lower frequency range.

Fig. 5 presents the harmonic instability phenomenon caused by the interactions between the inner ACC loops of the three paralleled VSCs. In the test, the PLLs used with VSCs are tuned with a sufficiently low bandwidth in order to avoid the sideband harmonics shown in Fig. 4. The bandwidth of the ACC loop is increased from $f_s/20$ to $f_s/15$ at the time instant of T_i. The control bandwidth of $f_s/15$ was designed for a stable ACC loop with the single grid-connected VSC. However, it is clear that the three paralleled VSCs become unstable with the bandwidth of $f_s/15$. This ACC-induced harmonic instability problem has been well studied recently. In this case, the equivalent grid impedance for each single VSC is increased with the number of the paralleled VSCs, which tends to shift the passive LC resonance frequency to the frequency range where the negative damping is added by the time delay of the ACC loop [40].

Fig. 6 shows the measured result for the sideband-harmonic instability of the switching frequency, which occurs in the two paralleled VSCs using asynchronous carries [14]. Differing from Figs. 4 and 5, both the VSC output currents and the current

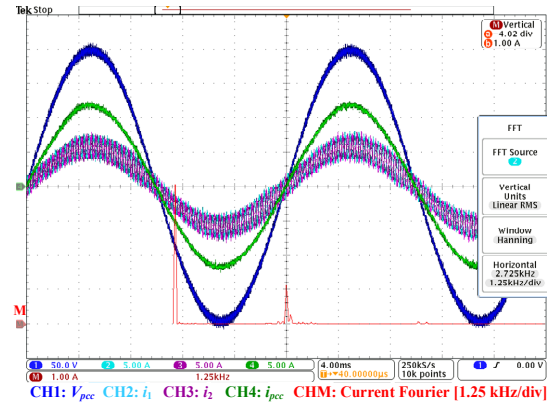

(a)

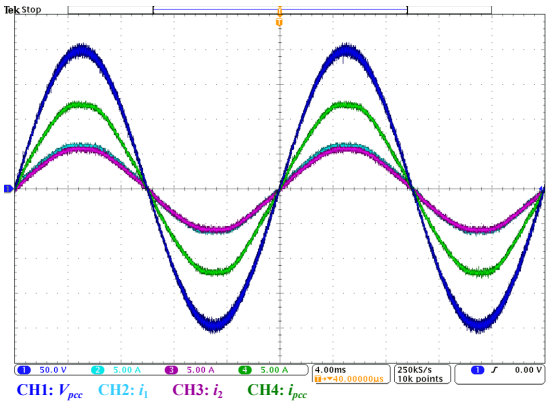

(b)

Fig. 6. Measured waveforms of the sideband (f_s) harmonic instability caused by the asynchronous carriers of the PWM. (a) Asynchronous carriers. (b) Synchronous carriers [14].

injected from the Point of Common Coupling (PCC) to the grid are shown. From Fig. 6(a), it is interesting to see that the current injected in the grid, i.e. the sum of the VSC output currents, is kept sinusoidal, whereas the VSC output currents are distorted with a high frequency (2.75 kHz) harmonic component. Yet, when the carriers of VSCs are intentionally synchronized, the VSC output currents become sinusoidal, as shown in Fig. 6(b). This sideband oscillation is induced by the additional sideband of the PWM [38], when accounting the perturbation frequency component into the modulating reference. Therefore, unlike the harmonic instability demonstrated in Figs. 4 and 5, this PWM-induced sideband oscillation cannot be predicted by means of conventional state-space averaging models of VSCs. Instead, the multiple-frequency small-signal models need to be used.

III. Linearized Modeling of Converters

The linearized modeling of electronic power converters is critical for revealing the causes of harmonic instability in power electronic based power systems. This section elaborates first the dynamic properties of power converters, and then discusses the basic procedure and adequacy of the typical modeling methods.

A. Dynamic Properties of Converters

Power converters are nonlinear and time-varying dynamical systems, where the nonlinearity is due to the dynamically varied duty cycle (control input of the modulator) with the closed-loop control system, and the time variance results from the switching modulation process and the time-periodic operating trajectories of ac systems [41], [42]. As for a power converter operating with a predefined switching function, the system is linear but time varying. However, if the switching modulation process can be neglected and the ac operating trajectory can be transformed as dc operating point in the *dq*-frame, the ac-dc converter will be nonlinear but time-invariant.

On the other hand, power converters are also hybrid systems of continuous dynamics of passive elements and discrete events of switching power semiconductor devices. Thus, there are two general ways to characterize the dynamics of power converters [43], i.e. the sampled-data model for extracting discrete-time dynamics of converters [44], and the continuous dynamic model based on the averaging techniques [19], [22].

Fig. 7 outlines the commonly used modeling methods for ac-dc converters, e.g. VSCs, and their basic modeling procedures and dynamic properties. First, the converter is represented by a switching model by assuming the ideal switching behaviors of power semiconductor devices. Then, three different approaches can be adopted for obtaining the continuous dynamic models of converters: 1) the state-space averaging approach based on the moving average operator, 2) the generalized averaging method, and 3) the HSS model. The modeling adequacy and constraints of these three methods are discussed as follows, and it points out that the linearized models obtained from these methods can be unified by the Harmonic Transfer Function (HTF) concept [9], [45]. The HTF is a MIMO transfer function matrix, which is Linear Time-Invariant (LTI) yet extracts the cross coupling dynamics between the input and output vectors (with multiple frequency components) of an LTP system [9]. It also shows that the *dq*-frame LTI model of balanced three-phase converters is mathematically equivalent to a 2nd-order HTF model [11].

B. State-Space Averaging (Moving Average)

The state-space averaging approach was first developed for dc-dc power converters, where the switching ripples are filtered out by applying the below moving average operator to the state variables of the converter [19].

$$\bar{x}(t) = \frac{1}{T}\int_{t-T}^{t} x(\tau)d\tau \tag{1}$$

where $T = 2\pi/\omega_s$, ω_s is the switching frequency of the converter. The averaged models of dc-dc converters are nonlinear but time invariant with the defined dc operating points. The Taylor series expansion can then be applied to obtain the LTI model.

In contrast, the averaged models of ac-dc converters are still nonlinear and time varying, due to the time-periodic operating trajectory of the ac system [42]. Moreover, the averaged models based on the moving average operator are merely adequate for the frequencies below half the switching frequency [19]. Three modeling approaches have been developed for linearizing the state-space averaging models of ac-dc converters:

1) DQ-frame model for balanced three-phase systems

In balanced three-phase systems, the time-periodic operating

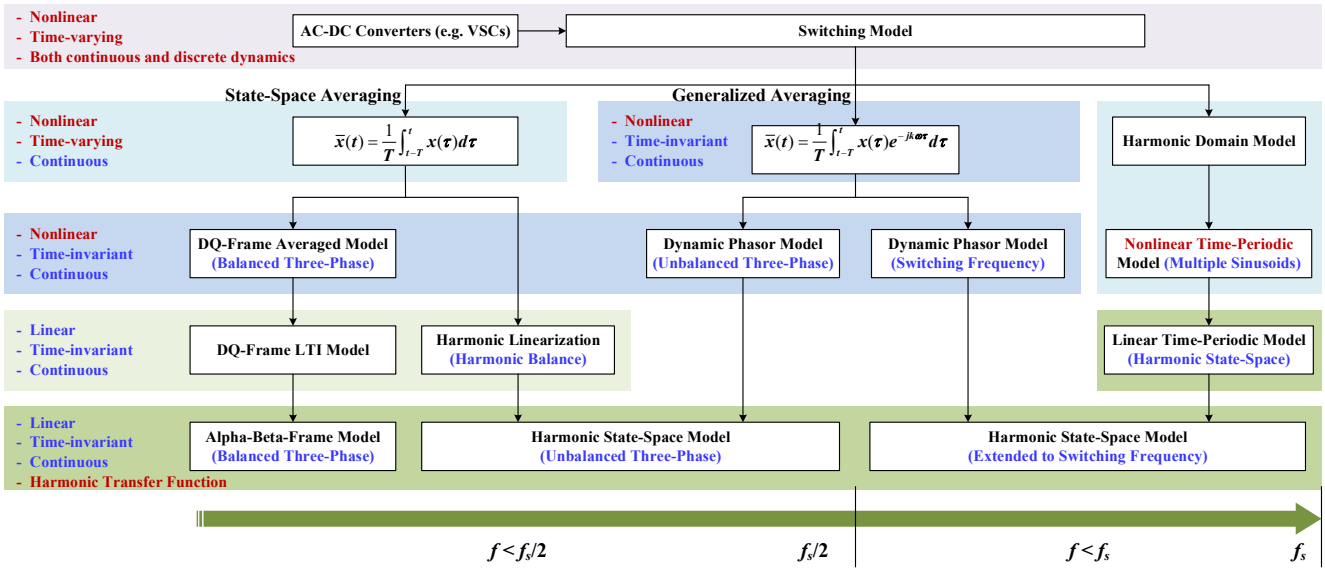

Fig. 7. Linearized modeling methods for ac-dc converters and their modeling procedure. f_s: switching frequency; LTI: Linear Time-Invariant;

trajectory can be transformed as the dc operating point by using the Park transformation [46]. Thus, the averaged models for the balanced three-phase converter systems can be transformed into nonlinear but time-invariant models in the *dq*-frame [47], which can then be, similarly to dc-dc converters, linearized around the defined dc operating point. Yet, it is worth noting that the Park transformation not only enables to obtain time-invariant models for balanced three-phase ac-dc converters, but also accounts for the frequency coupling dynamics (i.e. the sideband oscillations) of the fundamental frequency by using real space vectors. The frequency coupling dynamics are caused by either the inherent frequency transformation mechanism of ac-dc converters [42], or the asymmetrical *dq*-frame control dynamics of the PLL (*q*-axis), the DVC (*d*-axis) and AVC (*q*-axis) loops [48], [49], as shown in Fig. 2.

2) Harmonic linearization method

Alternatively, the LTI model of ac-dc converters can also be obtained by using the harmonic linearization method [27], [50]. The approach is based on the principle of harmonic balance and the describing function method [51]. As illustrated in Fig. 7, the phase-domain state-space averaging model, which is nonlinear and time varying, is linearized directly by superimposing with two sinusoidal perturbations: one perturbation is in the positive sequence and the other is in the negative sequence [27]. Then, the Fourier analysis is applied to the output and the components at the perturbation frequency are extracted in order to formulate the LTI transfer function model in the frequency domain.

Unlike the *dq*-frame LTI model, the model developed by the harmonic linearization approach is in the sequence domain, and there is no need to transform the model into a nonlinear but time-invariant system. However, the cross-coupling dynamics between the sequence components are overlooked [50], which fails to characterize the frequency-coupling dynamics of ac-dc converters and leads to inaccurate stability prediction [11], [52]. Moreover, in the balanced three-phase systems, the frequency-coupling nature of ac-dc converters may not necessarily cause the negative-sequence component, which will be elaborated in details in the following.

3) Alpha-beta-frame model for balanced three-phase system

Capturing the frequency-coupling (sideband) oscillations of the fundamental frequency is thus critical for linearized models of ac-dc converters. The *dq*-frame LTI model accounts for the frequency-coupling dynamics using a 2nd-order tensor (a 2×2 matrix) in an orthogonal coordinate [53]. Yet, it does not reveal the coupled component and their cross-coupling dynamics for a given input vector. Thus, a frequency-coupling model in the phase domain (the *αβ*-frame) is recently proposed in [11]. The model is derived from the *dq*-frame model based on complex space vectors and complex transfer functions [54]. Yet, it shows the frequency-coupling relationship between the asymmetrical *dq*-frame model and its equivalent in the *αβ*-frame.

Considering a general *dq*-frame model for a balanced three-phase converter, which is given by the transfer function matrix:

$$\begin{bmatrix} y_d \\ y_q \end{bmatrix} = G_{dq}(s)\begin{bmatrix} u_d \\ u_q \end{bmatrix} = \begin{bmatrix} g_{dd}(s) & g_{dq}(s) \\ g_{qd}(s) & g_{qq}(s) \end{bmatrix}\begin{bmatrix} u_d \\ u_q \end{bmatrix} \tag{2}$$

where $[u_d \ u_q]^{\mathrm{T}}$ and $[y_d \ y_q]^{\mathrm{T}}$ denote the real space vectors for the input and output of the *dq*-frame model, respectively.

By the help of complex space vectors and complex transfer functions [54], the *dq*-frame model can be represented by [11]

$$\begin{bmatrix} \mathbf{y}_{\mathbf{dq}} \\ \mathbf{y}_{\mathbf{dq}}^{*} \end{bmatrix} = \begin{bmatrix} \mathbf{G}_{+}(s) & \mathbf{G}_{-}(s) \\ \mathbf{G}_{-}^{*}(s) & \mathbf{G}_{+}^{*}(s) \end{bmatrix}\begin{bmatrix} \mathbf{u}_{\mathbf{dq}} \\ \mathbf{u}_{\mathbf{dq}}^{*} \end{bmatrix} \tag{3}$$

where $\mathbf{u_{dq}}$ and $\mathbf{y_{dq}}$ are complex forms of the real space vectors $[u_d \ u_q]^{\mathrm{T}}$ and $[y_d \ y_q]^{\mathrm{T}}$, respectively, i.e. $\mathbf{u_{dq}} = u_d + ju_q$, $\mathbf{y_{dq}} = y_d + jy_q$. $\mathbf{u}_{\mathbf{dq}}^{*}$ and $\mathbf{y}_{\mathbf{dq}}^{*}$ are the complex conjugates of $\mathbf{u_{dq}}$ and $\mathbf{y_{dq}}$. $\mathbf{G}_{+}(s)$ and $\mathbf{G}_{-}(s)$ are the complex transfer functions derived from (2):

$$\mathbf{G}_{+}(s)=\frac{g_{dd}(s)+g_{qq}(s)}{2}+j\frac{g_{qd}(s)-g_{dq}(s)}{2}$$
$$\mathbf{G}_{-}(s)=\frac{g_{dd}(s)-g_{qq}(s)}{2}+j\frac{g_{qd}(s)+g_{dq}(s)}{2} \quad (4)$$

$\mathbf{G}_{+}^{*}(s)$ and $\mathbf{G}_{-}^{*}(s)$ are the complex conjugates of $\mathbf{G}_{+}(s)$ and $\mathbf{G}_{-}(s)$, respectively.

As for the symmetrical *dq*-frame model, where

$$g_d(s)=g_{dd}(s)=g_{qq}(s),\quad g_q(s)=-g_{dq}(s)=g_{qd}(s) \quad (5)$$

The complex equivalent of (3) is then simplified as [50]

$$\mathbf{y}_{\mathbf{dq}}=\mathbf{G}(s)\mathbf{u}_{\mathbf{dq}},\quad \mathbf{G}(s)=g_d(s)+jg_q(s) \quad (6)$$

where the complex transfer function $\mathbf{G}(s)$ facilitates the analysis with the Single-Input Single-Output (SISO) system tools, and it also reveals the frequency translation relationship between the symmetrical *dq*-frame model and its *αβ*-frame equivalent, i.e.

$$\mathbf{y}_{\alpha\beta}=\mathbf{G}(s-j\omega_1)\mathbf{u}_{\alpha\beta} \quad (7)$$

Hence, there is no frequency-coupling dynamics involved with the symmetrical *dq*-frame model.

Following the frequency translation relationship given in (7), the *αβ*-frame equivalent for the asymmetrical *dq*-frame model can be derived as [11]

$$\begin{bmatrix}\mathbf{y}_{\alpha\beta}\\ e^{j2\omega_1 t}\mathbf{y}_{\alpha\beta}^{*}\end{bmatrix}=\begin{bmatrix}\mathbf{G}_{+}(s-j\omega_1) & \mathbf{G}_{-}(s-j\omega_1)\\ \mathbf{G}_{-}^{*}(s-j\omega_1) & \mathbf{G}_{+}^{*}(s-j\omega_1)\end{bmatrix}\begin{bmatrix}\mathbf{u}_{\alpha\beta}\\ e^{j2\omega_1 t}\mathbf{u}_{\alpha\beta}^{*}\end{bmatrix} \quad (8)$$

Compared to (7), it is evident in (8) that a frequency-coupling term at the frequency $2\omega_1-\omega$ is generated by the asymmetrical *dq*-frame model, given an input at the frequency ω. Hence, even in balanced three-phase converter systems, there is a frequency-coupling mechanism introduced by the asymmetrical dynamics in the *dq*-frame. The input component of (8) at the frequency ω may be external disturbances at the dc- or ac-side [55], or may result from the internal oscillations of the PLL and the outer control loops [11]-[13], [48]-[50]. Moreover, for the balanced three-phase ac-dc converters, the negative-sequence component can only be introduced when $\omega > 2\omega_1$. The sequence-domain model cannot predict the frequency coupling term when $\omega < 2\omega_1$. Yet, this fact is overlooked in the conventional sequence-domain model. In addition, the transfer function matrix given in (8) is a 2nd-order HTF, which is itself LTI yet captures the frequency-coupling dynamics of an LTP system [9], [45].

C. Multiple-Frequency Model

From the above discussions, it can be seen that the balanced three-phase converter systems can be accurately modeled either by a 2nd-order transfer function matrix in the *dq*-frame, or by a 2nd-order HTF in the *αβ*-frame. However, for the unbalanced three-phase converter systems, more frequency-coupling terms need to be considered, which are corresponding to the positive-sequence and negative-sequence components of the ac system. Instead of the dual-frequency model given in (8), the multiple-frequency modeling approach is required to capture the cross-coupling dynamics between those components.

There have been two general multiple-frequency modeling methods developed for unbalanced three-phase systems, which are the generalized averaging method [22], [23], also known as the dynamic phasor [56]-[58], and the HSS model [9], [24], [45], [59]. Both methods are based on the truncated Fourier series and the multiple-input describing function [51], [60], and their difference lies in how to transform the discrete switching events into a continuous dynamic model.

1) Generalized averaging and dynamic phasor

The generalized averaging method was earlier introduced to capture the dynamic of the switching-frequency component for dc-dc converters [22]. In the approach, a time-varying Fourier coefficient is defined as given below:

$$\langle x\rangle_k(t)=\frac{1}{T}\int_{t-T}^{t}x(\tau)e^{-jk\omega_s T}d\tau \quad (9)$$

Based on this operator, two Fourier coefficients can be derived for dc-dc converters, i.e. $k = 0$ representing the dc component, which is the same as the moving average operator given in (1), and $k = 1$ that denotes the Fourier coefficient of the switching-frequency ac component [23]. The latter Fourier coefficient (i.e. $k = 1$) is a complex vector expressed in the *dq*-frame rotating at the switching frequency. Thus, the obtained multiple-frequency averaged model is nonlinear but time-invariant, due to the well-defined operating point for the *dq*-frame complex vector. Two equations are formulated to characterize the multiple-frequency dynamics [22]:

$$\frac{d\langle x\rangle_k(t)}{dt}=\left\langle\frac{dx}{dt}\right\rangle_k(t)-jk\omega_s\langle x\rangle_k(t) \quad (10)$$

$$\langle xy\rangle_k=\sum_i\langle x\rangle_{k-i}\langle y\rangle_i \quad (11)$$

The generalized averaging operator has also been extended to model the single-phase and unbalanced three-phase electrical systems [56]-[58], where the time-varying Fourier coefficients of the positive-sequence and negative-sequence components are extracted, which are also named as dynamic phasors [57]. The cross couplings between the sequence components can be captured by (11). Unlike the state-space averaging model [46], which is nonlinear and time varying, the dynamic phasor model is time invariant in multiple reference (*dq*-) frames. On the other hand, the dynamic phasor model is different from the multiple-reference-frame model [61], where the cross couplings between different quantities are overlooked [56].

For linearization, the small-signal perturbations are imposed on the equilibrium points of dynamic phasors [60], where the frequency-coupling dynamics among the variables in different *dq*-frames can then be modeled by following the transformation from (2) to (8). Consequently, a higher-order HTF is established for the unbalanced three-phase ac-dc converters.

Besides the dynamic phasors for the sequence components, the higher-order harmonic interactions of ac-dc converters can also be accounted by the generalized averaging operator, which

are known as the extended harmonic domain model [62], [63]. However, in those methods, the converter control dynamics are overlooked, i.e. only the converter with a predefined modulator, which is essentially an LTP system, is modeled [64].

2) HSS method

The HSS method was originally developed for analyzing the dynamics of helicopter blades [45], and was later applied to deal with the harmonic stability of locomotive inverter systems [9]. The core idea of the HSS is to establish an analogy to the LTI state-space model for LTP dynamic systems, which is achieved by introducing an Exponentially Modulated Periodic (EMP) signal representation [45], which is given by

$$x(t) = \sum_k x_k(t) e^{jk\omega_s t} = \sum_k X_k(s) e^{st} e^{jk\omega_s t} \tag{12}$$

$$\dot{x}(t) = \sum_k (s + jk\omega_s) X_k(s) e^{(s+jk\omega_s)t} \tag{13}$$

where the term 'e^{st}', $s = \sigma + j\omega$ is used to modulate the Fourier coefficients for extracting the transient responses of harmonic components. Hence, similarly to (9), the EMP representation also defines the time-varying coefficients of the Fourier series expansion of the system variables. However, instead of directly defining the coefficients for the LTP system, the coefficients of dynamic phasors are derived by integrating the system variables over a moving time window.

Besides the representation of system variables, the modeling procedure of the HSS approach is different from the generalized averaging models. As illustrated in Fig. 7, the switching model of converters is first decomposed into the harmonic domain with the steady-state time-periodic operating trajectories [9]. Then, the resulting nonlinear time periodic model is linearized directly in the neighborhood of the time-periodic operating trajectories, leading to an LTP model, which is given by

$$\begin{aligned} \Delta\dot{\mathbf{x}}(t) &= \mathbf{A}(t)\Delta\mathbf{x}(t) + \mathbf{B}(t)\Delta u(t) \\ \Delta y(t) &= \mathbf{C}(t)\Delta\mathbf{x}(t) + \mathbf{D}(t)\Delta u(t) \end{aligned} \tag{14}$$

where $\mathbf{A}(t)$, $\mathbf{B}(t)$, $\mathbf{C}(t)$, $\mathbf{D}(t)$ are time-periodic matrices, $\Delta\mathbf{x}(t)$ is the state vector of the system, $\Delta u(t)$ and $\Delta y(t)$ are the input and output variables, respectively. Next replacing these matrices by their Fourier series [64], e.g.

$$\mathbf{A}(t) = \sum_k \mathbf{A}_k e^{jk\omega_s t} \tag{15}$$

and substituting $\Delta\mathbf{x}(t)$, $\Delta u(t)$ and $\Delta y(t)$ by their respective EMP forms in (12), (13), the HSS model is obtained as

$$\begin{aligned} (s + jk\omega_s)\mathbf{X}_k(s) &= \sum_n \mathbf{A}_{k-n}\mathbf{X}_n(s) + \sum_n \mathbf{B}_{k-n}U_n(s) \\ Y_k(s) &= \sum_n \mathbf{C}_{k-n}\mathbf{X}_n(s) + \sum_n \mathbf{D}_{k-n}U_n(s) \end{aligned} \tag{16}$$

Thus, the LTP system is represented by an MIMO state-space model, similar to the LTI state-space model. Based on (16), the HTF can then be derived as [59]

$$\mathbf{Y}(s) = \mathbf{H}(s)\mathbf{U}(s) \Rightarrow$$

$$\mathbf{H}(s) = \begin{bmatrix} \ddots & \vdots & & \iddots \\ & H_0(s - j\omega_s) & H_{-1}(s) & H_{-2}(s + j\omega_s) & \\ \cdots & H_1(s - j\omega_s) & H_0(s) & H_{-1}(s + j\omega_s) & \cdots \\ & H_2(s - j\omega_s) & H_1(s) & H_0(s + j\omega_s) & \\ \iddots & \vdots & & \ddots \end{bmatrix} \tag{17}$$

$$\begin{aligned} \mathbf{Y}(s) &= \begin{bmatrix} \cdots & Y_{-1}(s) & Y_0(s) & Y_1(s) & \cdots \end{bmatrix}^T \\ \mathbf{U}(s) &= \begin{bmatrix} \cdots & U_{-1}(s) & U_0(s) & U_1(s) & \cdots \end{bmatrix}^T \end{aligned} \tag{18}$$

Hence, the HTF derived from the HSS model provides a unified multiple-frequency model for ac-dc converters. Yet, instead of linearizing the system on the operating point in the generalized averaging model, the HSS method linearizes the system around the time-periodic operating trajectories [64].

Table I summarizes the adequacies of the different modeling methods for analyzing the harmonic instability issues under the different system conditions. All the models are adequate for the analysis of harmonic instability induced by the interactions of current control loops. While the harmonic linearization method considers the negative-sequence component, it does not extract the cross-coupling dynamics.

IV. System Stability Analysis

Two analytical methods have been developed for the system-level stability analysis, which are the eigenvalue analysis based on the state-space model of the system in the time domain, and the impedance-based analysis based on the transfer functions of components in the frequency domain.

A. Eigenvalue Analysis

The eigenvalue analysis has become a common practice for analyzing the small-signal stability of legacy power grids. The method is developed based on the state-space representation of the power system, which is, after the small-signal linearization, given by [25]

$$\begin{aligned} \Delta\dot{\mathbf{x}} &= \mathbf{A}\Delta\mathbf{x} + \mathbf{B}\Delta\mathbf{u} \\ \Delta\mathbf{y} &= \mathbf{C}\Delta\mathbf{x} + \mathbf{D}\Delta\mathbf{u} \end{aligned} \tag{19}$$

where **A**, **B**, **C**, **D** are the time-invariant matrices for the LTI system, and the eigenvalues of the state matrix **A** arderived by

$$\det(s\mathbf{I} - \mathbf{A}) = 0 \tag{20}$$

which is also the characteristic equation of the LTI system. The eigenvalues indicate the dynamic modes of the power system. In addition, the eigenvectors also have important implications on the power system dynamics. The right eigenvectors reveal the distribution of dynamic modes through state variables, and the left eigenvector identifies the relative effects of the different initial conditions of state variables on dynamic modes [65]. The combination of these two eigenvectors leads to the participation factor [66], which weighs the participation of state variables in the dynamic modes. Hence, the dynamic analysis based on the eigenvalues and eigenvectors not only captures the input-output

TABLE I
MODELING ADEQUACIES OF DIFFERENT MODELING METHODS FOR HARMONIC STABILITY ANALYSIS

Modeling Adequacy	DQ-Frame LTI Model	Harmonic Linearization	Alpha-beta-Frame Model	Dynamic Phasor Model	Harmonic State-Space Model
Frequency-coupling dynamics	+	–	+	+	+
Sideband (f_1) harmonic stability	+	–	+	+	+
Harmonic stability - current control	+	+	+	+	+
Sideband (f_s) harmonic stability	–	–	–	+	+
Unbalanced three-phase/single-phase	–	+	–	+	+

dynamics of the system, but provides also a global view on the modes of responses and the relative effects of state variables.

The small-signal stability of conventional power systems are dominated by the electromechanical dynamics of synchronous generators. The electromagnetic transients of electric networks are often overlooked in the state-space model, except the study of sub-synchronous resonances [66]. The well-decoupled time constants of generator- and network-dynamics facilitates using the closed-form eigenvalue analysis for large-scale power grids. Nevertheless, the harmonic stability of power electronic based power systems feature multi-timescale and frequency-coupling dynamics, which lead to oscillations in a wide frequency range, as shown in Fig. 2. The wide frequency range of oscillations are tightly coupled with the electric network dynamics, leading to a very high-order system state matrix [67], which consequently imposes a high computational burden for the stability analysis. Moreover, in order to capture the frequency-coupling dynamics of unbalanced three-phase power systems, the HSS models of ac-dc converters are required, which also complicates the model derivation process with the increased system order [68].

To address the high computational demand for deriving the state-space model, the Component Connection Method (CCM) was reported for converter-based power grids in [69]. The CCM presents a computationally efficient procedure for deriving the LTI state-space model given in (19). Fig. 8 shows a comparison between the modeling procedures of the general state-space representation and the CCM. In the CCM, the power system is decomposed into multiple components, e.g. power converters, generators, and the electric network, which are interconnected by linear algebraic relationships defined by their interfaces [70]. Then, the components are linearized locally, and their LTI state-space models constitute a composite component model, which is given by

$$\begin{aligned} \Delta\dot{\mathbf{x}} &= \mathbf{F}\Delta\mathbf{x} + \mathbf{H}\Delta\mathbf{a} \\ \Delta\mathbf{b} &= \mathbf{J}\Delta\mathbf{x} + \mathbf{K}\Delta\mathbf{a} \end{aligned} \tag{21}$$

where the state matrix $\mathbf{F}$ is a diagonal matrix of state matrices of components, i.e. $\mathbf{F} = \text{diag}\{\mathbf{F}_1, \mathbf{F}_2, \ldots \mathbf{F}_n\}$, and $\mathbf{H}$, $\mathbf{J}$, $\mathbf{K}$ follows the similar form. $\mathbf{a}$ and $\mathbf{b}$ are the vectors of the input and output variables of components.

The interconnections of the components are defined by [69]

$$\begin{aligned} \mathbf{a} &= \mathbf{L}_{11}\mathbf{b} + \mathbf{L}_{12}\mathbf{u} \\ \mathbf{y} &= \mathbf{L}_{21}\mathbf{b} + \mathbf{L}_{22}\mathbf{u} \end{aligned} \tag{22}$$

where $\mathbf{u}$ and $\mathbf{y}$ are the input and output vectors of the system. The matrices $\mathbf{L}_{ij}$ are linear algebraic, which depends on how to define the input and output of components. Combining (21) and (22) leads to the state-space model given in (19). The prominent features of the CCM are the modularity and scalability for large-scale power systems. The linear algebraic interconnections of the components significantly reduces the computational efforts.

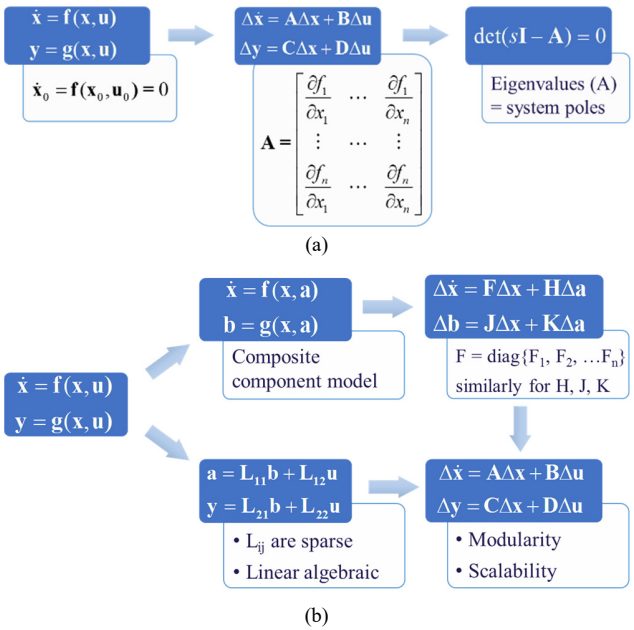

Fig. 8. Comparison between the modeling procedures of the general state-space representation and Component Connection Method (CCM). (a) General state-space model. (b) CCM-based model.

It is worth noting that the state-space models of components can also be represented by transfer functions, where the inputs and outputs can be defined in a similar way to the impedance-based models [17]. A frequency-domain CCM-based model can thus be obtained with the frequency scanning (i.e. the black box modeling) technique, which can be analyzed either in a closed-form (MIMO transfer function matrices) based on system poles [71] or with the impedance-based analysis [17], which will be discussed next.

B. Impedance-Based Analysis

The impedance-based method was originally developed for the design-oriented analysis of input filters for dc-dc converters [29]. In that work, a minor feedback loop is introduced, which consists of the input impedance of the converter and the output impedance of the LC-filter, and the impedance ratio defines the loop gain. Thus, the Nyquist stability criterion can be applied to characterize the dynamic effect of the input LC-filter resonance. The concept of minor feedback loop was later extended for the stability analysis of dc power systems for spacecraft [72], where the minor feedback loop comprises the impedances of multiple

converters, and the impedance ratio characterizes the dynamic interactions of converters. In [30], the impedance-based method was applied to analyze the stability of ac power systems, and the generalized Nyquist stability criterion was used to evaluate the MIMO transfer function matrices, owing to the frequency-coupling dynamics of ac-dc converters.

Fig. 9 elaborates the basic principle of the impedance-based analysis method. A converter-based power system that consists of voltage-controlled and current-controlled ac-dc converters is represented by the impedance equivalent, where the converters are modeled by the Norton (current-controlled converters) and Thevenin (voltage-controlled converters) equivalent circuits, as shown in Fig. 9 (a). It is interesting to note that the impedance-based approach is similar to the CCM, where the system model is also formed based on the models of components, and thus it keeps the advantages of modularity and scalability as in the case of the CCM. However, instead of identifying the eigenvalues of the system, the impedance-based approach predicts the system stability locally at the point of connection of each converter, where the rest of the system is equivalent to an impedance seen from the converter.

Fig. 9(b) depicts a general impedance equivalent model for characterizing the converter-system interaction, from which the minor feedback loops for the current-controlled and voltage-controlled converter can be derived, which are depicted in Figs. 9(c) and 9(d), respectively. Both the current-controlled and the voltage-controlled converters lead to the same minor feedback loop, where the loop gain is the impedance ratio, i.e. $Y_c(s)Z_s(s)$. Thus, the system stability can then be evaluated by

$$i_o(s)=\frac{1}{1+Y_c(s)Z_s(s)}i_c(s)+\frac{Y_c(s)}{1+Y_c(s)Z_s(s)}V_s(s) \tag{23}$$

$$V_o(s)=\frac{1}{1+Y_c(s)Z_s(s)}V_s(s)+\frac{Z_s(s)}{1+Y_c(s)Z_s(s)}i_c(s) \tag{24}$$

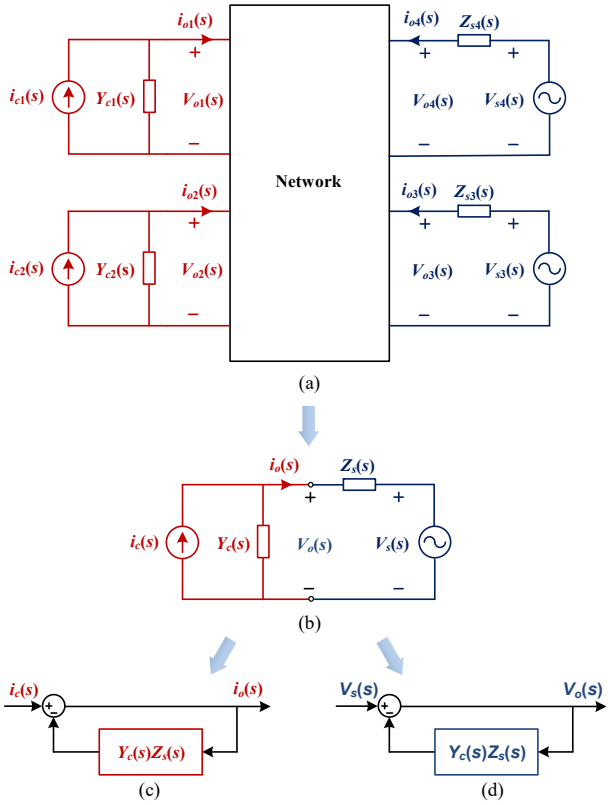

Fig. 9. Basic principle of the impedance-based stability analysis method. (a) Impedance-based model of a converter-based power system. (b) General impedance equivalent derived for each converter. (c) Minor feedback loop for current-controlled converters. (d) Minor feedback loop for voltage-controlled converters.

C. Comparison of Stability Analysis Tools

Table II presents a comparison between the basic state-space representation, the CCM, and the impedance-based analysis, on a number of features. Compared to the eigenvalue analysis, the superior feature of the impedance-based approach is the black-box modeling, i.e. the impedance profiles of converters and the electric network can be measured with the frequency scanning technique, which was earlier used for the prediction of the sub-synchronous oscillations in the legacy power systems [65]. This feature is particularly attractive for analyzing the interactions of multiple converters provided by the different vendors. Further, compared to the CCM, the impedance models provide physical insights into the effects of controllers on the terminal behaviors of converters, and it facilitates a design-oriented analysis [29].

By utilizing the nodal admittance matrix [17], the frequency-domain impedance analysis is more computationally efficient than the basic state-space representation, and can be scalable to different scales of power systems [73]. However, the transfer functions can merely predict the input-output dynamics at the converter terminal, i.e. how a single converter interacts with the rest of the system. The effects of state variables on the stability margin of the system are not identified, and consequently the system oscillation modes with different damping levels cannot be observed in the frequency domain [74].

In addition, the dynamic interactions of the rest subsystems may bring RHP poles/zeros into the equivalent impedance seen from the converter [30], [31], [75]. The presence of RHP poles may give rise to an inaccurate stability implication [31], while the presence of RHP zeros may yield incorrect impedance specifications for the active stabilization [30], [75]. Thus, the RHP poles/zeros impose constraints on the system partitioning and the aggregation of impedances of subsystems.

In contrast, the CCM not only preserves the modularity and the scalability of the impedance method, but also overcomes the drawbacks on the identification of system oscillation modes and the participation factors of state variables. However, owing to the state-space representation of the CCM, it requires a prior knowledge of the system parameters and control structures [69]. Thus, the CCM cannot be readily used to analyze the interaction between converters from multiple vendors. Moreover, the CCM merely simplifies the computation procedure for obtaining the state-space model of the system. The eigenvalue-based stability analysis still requires higher computational resources than the frequency-domain impedance method. The dynamic reduction techniques based on a subset of oscillation modes have been developed for the efficient analysis [26], yet its effectiveness on the analysis of sideband oscillations needs to be further studied.

TABLE II
COMPARISON OF SYSTEM STABILITY ANALYSIS TOOLS

Features	Basic State-Space Representation	Component Connection Method (CCM)	Impedance-Based Analysis
Identification of dynamic modes	+	+	–
Participation factors of state variables	+	+	–
Input-output dynamics	+	+	+
Design-oriented analysis	Moderate	Moderate	High
Black-box modeling (frequency-scanning)	–	–	+
Modularity	–	+	+
Scalability	Low	High	High

V. FUTURE TRENDS AND CONCLUSIONS

This paper has discussed the concept and phenomena of the harmonic stability in the modern power electronic based power systems. It has been pointed out that the harmonic stability is in essential a breed of small-signal stability, yet it is used to denote the sideband oscillations around the fundamental frequency and the switching frequency of converters, as well as the resonances induced by the wideband control dynamics of converters. It has also been emphasized that the frequency-coupling small-signal models of converters are important for the harmonic stability analysis. It has been revealed that the HTF obtained from the LTP system theory yields a unified model of ac-dc converters. The challenges with the system stability analysis have also been discussed. To address the challenges, more research efforts on the following topics are expected:

1) Adequate small-signal modeling of power converters, which is dependent on the system conditions and the concerned instability phenomena.
2) An effective system analysis tool, which can identify the oscillation modes for multiple converters provided by different vendors, is demanded.
3) The system partitioning methods and dynamic model aggregation techniques are urgently demanded for the stability analysis of very large power electronic based power systems.

VI. REFERENCES

[1] F. Blaabjerg, Y. Yang, D. Yang, and X. Wang, "Distributed power generation and protection," *Proc. IEEE*, vol. 105, no. 7, pp. 1311-1331, Jul. 2017.

[2] B. Ferreira, "Understanding the Challenges of Converter Networks and Systems: Better opportunities in the future," *IEEE Power Electronics Mag.*, vol. 3, no. 2, pp. 46-49, Jun. 2016.

[3] B. Kroposki, *et al*., "Achieving a 100% renewable grid: operating electric power systems with extremely high levels of variable renewable energy," *IEEE Power & Energy Mag.* vol. 15, no. 2, pp. 61-73, Mar./Apr. 2017.

[4] F. Blaabjerg, R. Teodorescu, M. Liserre and A. V. Timbus, "Overview of control and grid synchronization for distributed power generation systems," *IEEE Trans. Ind. Electron.*, vol. 53, no. 5, pp. 1398-1409, Oct. 2006.

[5] L. Harnefors, X. Wang, A. G. Yepes and F. Blaabjerg, "Passivity-based stability assessment of grid-connected VSCs - an overview," *IEEE J. Emerg. Sel. Topics Power Electron.*, vol. 4, no. 1, pp. 116-125, Mar. 2016.

[6] R. Turner, S. Walton, and R. Duke, "A case study on the application of the Nyquist stability criterion as applied to interconnected loads and sources on grids," *IEEE Trans. Ind. Electron*., vol. 60, no. 7, pp. 2740-2749, Jul. 2013.

[7] C. Buchhagen, M. Greve, A. Menze, and J. Jung, "Harmonic stability – practical experience of a TSO," in *Proc. Wind Integration Workshop*, 2016, pp. 1-6.

[8] C. Li, "Unstable operation of photovoltaic inverter from field experiences," *IEEE Trans. Power Del.*, vol. PP, no. 99, pp. 1-1.

[9] E. Mollerstedt and B. Bernhardsson, "Out of control because of harmonics – An analysis of the harmonic response of an inverter locomotive," *IEEE Control Syst. Mag.,* vol. 20, no. 4, pp. 70-81, Aug. 2000.

[10] X. Wang, F. Blaabjerg, and P. C. Loh, "Passivity-based stability analysis and damping injection for multiparalleled VSCs with LCL filters," *IEEE Trans. Power Electron*., vol. 32, no. 11, pp. 8922-8935, Nov. 2017.

[11] X. Wang, L. Harnefors, and F. Blaabjerg, "Unified impedance model of grid-connected voltage-source converters," *IEEE Trans. Power Electron.*, vol. 33, no. 2, pp. 1775-1787, Feb. 2018.

[12] J. Zhou, H. Ding, S. Fan, Y. Zhang, and A. M. Gole, "Impact of short-circuit ratio and phase-locked loop parameters on the small-signal behavior of a VSC-HVDC converter," *IEEE Trans. Power Del.*, vol. 29, no. 5, pp. 2287-2296, Oct. 2014.

[13] N. Bottrell, M. Prodanovic, and T. C. Green, "Dynamic stability of a microgrid with an active load," *IEEE Trans. Power Electron.*, vol. 28, no. 11, pp. 5107-5119, Nov. 2013.

[14] D. Yang, X. Wang, and F. Blaabjerg, "Sideband-harmonic instability of paralleled inverters with asynchronous carriers," *IEEE Trans. Power Electron.*, vol. 33, no. 6, pp. 4571-4577.

[15] L. Harnefors, R. Finger, X. Wang, H. Bai, and F. Blaabjerg, "VSC input-admittance modeling and analysis above the Nyquist frequency for passivity-based stability assessment," *IEEE Trans. Ind. Electron.,* vol. 64, no. 8, pp. 6362-6370, Aug. 2017.

[16] A. Paice and M. Meyer, "Rail network modeling and stability: the input admittance criterion," in *Proc. 14th Int. Symp. Math. Theory Netw. Syst.,* 2000, pp. 1-6.

[17] X. Wang, F. Blaabjerg, and W. Wu, "Modeling and analysis of harmonic stability in ac power-electronics-based power system," *IEEE Trans. Power Electron*., vol. 29, no. 12, pp. 6421-6432, Dec. 2014.

[18] F. Wang, J. L. Duarte, M. A. M. Hendrix, and P. F. Ribeiro, "Modeling and analysis of grid harmonic distortion impact of aggregated DG inverters," *IEEE Trans. Power Electron*., vol. 26, no. 3, pp. 786-797, Mar. 2011.

[19] G. W. Wester and R. D. Middlebrook, "Low-frequency characterization of switched dc-dc converters," *IEEE Trans. Aero. Electron. Syst.,* vol. AES-9, pp. 376-385, May 1973.

[20] R. D. Middlebrook, "Small-signal modeling of pulse-width modulated switched-mode power converters," *Proc. IEEE,* vol. 76, pp. 343-354, Apr. 1988.

[21] Y. Qiu, M. Xu, J. Sun, and F. C. Lee, "A generic high-frequency model for the nonlinearities in Buck converters," *IEEE Trans. Power Electron.*, vol. 22, No. 5, pp. 1970-1977, Sept. 2007.

[22] S. R. Sanders, J. M. Noworolski, X. Z. Liu and G. C. Verghese, "Generalized averaging method for power conversion circuits," *IEEE Trans. Power Electron.*,, vol. 6, no. 2, pp. 251-259, Apr. 1991.

[23] V. A. Caliskan, O. C. Verghese and A. M. Stankovic, "Multifrequency averaging of DC/DC converters," *IEEE Trans. Power Electron.*, vol. 14, no. 1, pp. 124-133, Jan. 1999.

[24] J. Kwon, X. Wang, F. Blaabjerg, C. L. Bak, A. R. Wood and N. R. Watson, "Harmonic instability analysis of single-phase grid connected converter using harmonic state space (HSS) modeling method", *IEEE Trans. Ind. Appl.*,, Vol. 52, No. 5, pp. 4188 – 4200. Sept./Oct. 2016,

[25] P. Kundur, *Power System Stability and Control*, New York: McGraw-Hill, 1994.

[26] Y. Wang, X. Wang, F. Blaabjerg, and Z. Chen, "Small-signal stability analysis of inverter-fed power systems using component connection method," *IEEE Trans. Smart Grid*, vol. PP, no. 99, pp. 1-1.

[27] J. Sun, "Small-signal methods for AC distributed power systems–a review," *IEEE Trans. Power Electron*., vol. 24, no. 11, pp. 2545-2554, Nov. 2009.

[28] J. Sun, "Impedance-based stability criterion for grid-connected inverters," *IEEE Trans. Power Electron*., vol. 26, no. 11, pp. 3075-3078, Nov. 2011.

[29] R. Middlebrook, "Input filter considerations in design and application of switching regulators," in *Proc. IEEE IAS'76*, 1976, pp. 366-382.

[30] M. Belkhayat. *Stability Criteria for AC Power Systems with Regulated Loads.* Ph.D. thesis, Purdue University, Dec. 1997.

[31] C. Yoon, X. Wang, C. L. Bak, and F. Blaabjerg, "Stabilization of multiple unstable modes for small-scale inverter-based power systems with impedance-based stability analysis," in *Proc. IEEE APEC* 2015, pp. 1202-1208.

[32] "Discussion on 'Harmonic instability between controlled static convertors and a.c. networks'," *Proc. Inst. Elect. Eng.*, vol. 114, no. 12, pp. 1925-1928, Dec. 1967.

[33] J. D. Ainsworth, "Harmonic instability between controlled static converters and a.c. networks," *Proc. Inst. Elect. Eng.*, vol. 114, pp.949-957, Jul. 1967.

[34] A. G. Phadke and J. H. Harlow, "Generation of abnormal harmonics in high-voltage ac-dc power systems," *IEEE Trans. Power Apparat. Syst.*, vol. PAS-87, no. 3, Mar. 1968.

[35] S. Chen, A. R. Wood, and J. Arrillaga, "HVDC converter transformer core saturation instability: a frequency domain analysis," *IEE Proc. Gen. Trans. Dis.*, vol. 143, no. 1, pp. 75-81, Jan. 1996.

[36] A. E. Hammad, "Analysis of second harmonic instability for the Chateauguay HVDC/SVC scheme," *IEEE Trans. Power Del.*, vol. 7, no. 1, Jan. 1992.

[37] L. Harnefors, "Analysis of subsynchronous torsional interaction with power electronic converters," *IEEE Trans. Power Syst.*, vol. 22, no. 1, pp. 305-313, Feb. 2007.

[38] H. Mouton, B. McGrath, D. G. Holmes, and R. H. Wilkinson, "One-dimensional spectral analysis of complex PWM waveforms using superposition," *IEEE Trans. Power Electron*., vol. 29, no. 12, pp. 6762-6778, Dec., 2014.

[39] X. Yue, F. Zhuo, S. Yang, Y. Pei and H. Yi, "A matrix-based multifrequency output impedance model for beat frequency oscillation analysis in distributed power systems," *IEEE J. Emerg. Sel. Topics Power Electron.*, vol. 4, no. 1, pp. 80-92, March 2016.

[40] M. Lu, X. Wang, P. C. Loh, and F. Blaabjerg, "Resonance interaction of multi-parallel grid-connected inverters with LCL filter," *IEEE Trans. Power Electron.*, vol. 32, no. 2, pp. 894-899, Feb. 2017.

[41] J. G. Kassakian, M. F. Schlecht, and G. C. Verghese, *Principles of Power Electronics*. Reading, MA: Addison-Wesley, 1991.

[42] A. R. Wood, D. J. Hume and C. M. Osauskas, "Linear analysis of waveform distortion for HVDC and FACTS devices," *in Proc. IEEE ICHQP* 2000, pp. 967-972.

[43] D. Maksimovic, A. M. Stankovic, V. J. Thottuvelil, and G. C. Verghese, "Modeling and simulation of power electronic converters," *Proc. IEEE,* vol. 89, pp. 898-912, Jun. 2001.

[44] G. C. Verghese, M. E. Elbuluk and J. G. Kassakian, "A general approach to sampled-data modeling for power electronic circuits," *IEEE Trans. Power Electron.*, vol. PE-1, no. 2, pp. 76-89, April 1986.

[45] N. M. Wereley, "Analysis and control of linear periodically time varying systems," Ph.D. dissertation, Dept. of Aeronautics and Astronautics, MIT, 1991.

[46] K. D. T. Ngo, "Low Frequency Characterization of PWM Converters," *IEEE Trans. Power Electron.,* vol. PE-1, pp. 223-230, Oct. 1986.

[47] S. Hiti, D. Boroyevich, and C. Cuadros, "Small-signal modeling and control of three-phase PWM converters," in *Proc. IEEE IAS* 1994, pp. 1143-1150.

[48] L. Harnefors, M. Bongiorno, and S. Lundberg, "Input-admittance calculation and shaping for controlled voltage-source converters," *IEEE Trans. Ind. Electron*., vol. 54, no. 6, pp. 3323-3334, Dec. 2007.

[49] B. Wen, D. Boroyevich, R. Burgos, P. Mattavelli, and Z. Shen, "Small-signal stability analysis of three-phase ac systems in the presence of constant power loads based on measured d-q frame impedances," *IEEE Trans. Power Electron.* vol. 30, no. 10, pp. 5952-5963, Dec. 2015.

[50] M. Cespedes and J. Sun, "Impedance modeling and analysis of grid-connected voltage-source converters," *IEEE Trans. Power Electron*. vol. 29, no. 3, pp. 1254-1261, Mar. 2014.

[51] A. Gelb and W. E. V. Velde, *Multiple-Input Describing Function and Nonlinear System Design*, New York: McGraw-Hill, 1968.

[52] M. K. Bakhshizadeh, X. Wang, F. Blaabjerg, J. Hjerrild, L. Kocewiak, C. L. Bak, and B. Hesselbaek, "Couplings in phase domain impedance moeling of grid-connected converters," *IEEE Trans. Power Electron.* vol. 31, no. 10, pp. 6792-6796, Oct. 2016.

[53] B. C. Smith, N. R. Watson, A. R. Wood, and J. Arrillaga, "Harmonic tensor linearisation of hvdc converters," *IEEE Trans. Power Del*. vol. 13, no. 4, pp. 1244-1250, Oct. 1998.

[54] L. Harnefors, "Modeling of three-phase dynamic systems using complex transfer functions and transfer matrices," *IEEE Trans. Ind. Electron*. vol. 54, no. 4, pp. 2239-2248, Aug. 2007.

[55] H. Yi, X. Wang, F. Blaabjerg, and F. Zhuo, "Impedance analysis of SOGI-FLL-based grid synchronization," *IEEE Trans. Power Electron.* vol. 32, no. 10, pp. 7409-7413, Oct. 2017.

[56] A. M. Stankovic, S. R. Sanders, and G. C. Verghese, "Dynamic phasors in modeling and analysis of unbalanced polyphaser ac machines," *IEEE Trans. Energy Conv.*, vol. 17, no. 1, pp. 107-113, Mar. 2002.

[57] P. Stefanov and A. M. Stankovic, "Modeling of UPFC operation under unbalanced conditions with dynamic phasors," *IEEE Trans. Power Syst.* vol. 17, no. 2, pp. 395-403, May 2002.

[58] A. M. Stankovic and T. Aydin, "Analysis of unbalanced power system faults using dynamic phasors," *IEEE Trans. Power Syst.*, vol. 15, no. 3, pp. 1062-1068, Aug. 2000.

[59] J. Kwon, X. Wang, F. Blaabjerg, C. L. Bak, A. R. Wood, and N. Watson, "Linearized modeling methods of ac-dc converters for an accurate frequency response," *IEEE J. Emerg. Sel. Topics Power Electron.*, vol. 5, no. 4, pp. 1526-1541, Dec. 2017.

[60] A. I. Mees, "Limit cycle stability," *J. Inst. Maths. Applics.*, vol. 11, pp. 281-295, 1973.

[61] S. D. Sudhoff, "Multiple reference frame analysis of unsymmetrical induction machines," *IEEE Trans. Energy Conv.*, vol. 8, no. 3, pp. 425-432, May 1993.

[62] J. Rico, M. Madrigal, and E. Acha, "Dynamic harmonic evolution using the extended harmonic domain," *IEEE Trans. Power Del*. vol. 18, no. 2, pp. 587-594, Apr. 2003.

[63] F. Yahyaie and P. W. Lehn, "On dynamic evaluation of harmonics using generalized averaging techniques," *IEEE Trans. Power Syst*. vol. 30, no. 5, pp. 2216-2224, Sept. 2015.

[64] S. Almer and U. Jonsson, "Harmonic analysis of pulse-width modulated systems," *Automatica*, vol. 45, no. 4, pp. 851-862, Apr. 2009.

[65] P. M. Anderson, B. L. Agrawal, and J. E. Van Ness, *Subsynchronous Resonance in Power Systems*, New York: IEEE Press, 1990.

[66] G. C. Verghese, I. J. Perezarriaga, and F. C. Schweppe, "Selective modal analysis with applications to electric power systems, part II: the dynamic stability problem," *IEEE Trans. Power Apparat. Syst.,* vol. PAS-101, pp. 3126-3134, Sept. 1982.

[67] N. Pogaku, M. Prodanovic, and T. C. Green, "Modeling, analysis and testing of an inverter-based microgrid," *IEEE Trans. Power Electron*., vol. 22, no. 2, pp. 613–625, Mar. 2007.

[68] V. Salis, A. Costabeber, S. M. Cox, and P. Zanchetta, "Stability assessment of power-converter-based ac systems by LTP theory: eigenvalue analysis and harmonic impedance estimation," *IEEE J. Emerg. Sel. Topics Power Electron.*, vol. PP, no. 99, pp. 1-1.

[69] G. Gaba, S. Lefebver, and D. Mukhedkar, "Comparative analysis and study of the dynamic stability of AC/DC systems," *IEEE Trans. Power Syst*., vol. 3, no. 3, pp. 978-985, Aug. 1988.

[70] S. Lefebver, "Tuning of stabilizers in multi-machine power systems," *IEEE Trans. Power Appar. Syst*., vol. PAS-102, no. 2, pp. 290-299, Feb. 1983.

[71] E. Ebrahimzadeh, F. Blaabjerg, X. Wang, and C. L. Bak, "Harmonic stability and resonance analysis in large PMSG-based wind power plants," *IEEE Trans. Sustain. Energy*, vol. 9, no. 1, pp. 12-23, Jan. 201.

[72] B. H. Cho and F. C. Lee, "Modeling and analysis of spacecraft power systems," *IEEE Trans. Power Electron*., vol. 3, no. 1, pp. 44-54, Jan. 1988.

[73] J. M. Undrill and T. E. Kostyniak, "Subsynchronous oscillations Part I – comprehensive stability analysis," *IEEE Trans. Power App. Syst.*, vol. PAS-95, no. 4, pp. 1446-1455, Jul./Aug. 1978.

[74] G. Gross, C. F. Imparato, P. M. Look, "A tool for the comprehensive analysis of power system dynamic stability," *IEEE Trans. Power App. Syst*., vol. PAS-101, no. 1, pp. 226-234, Jan. 1982.

[75] X. Wang, F. Blaabjerg, and P. C. Loh, "An impedance-based stability analysis method for paralleled voltage source converters," in *Proc. IEEE IPEC* 2014, pp. 1529-1535.